Electronically controlled agile lens-based broadband variable photonic delay line for photonic and radio frequency signal processing

Nabeel A. Riza,* Syed Azer Reza, and Philip J. Marraccini

Photonic Information Processing Systems Laboratory, The College of Optics and Photonics (CREOL), University of Central Florida, 4000 Central Florida Boulevard, Orlando, Florida 32816-2700, USA

*Corresponding author: riza@creol.ucf.edu

Received 12 July 2010; revised 20 October 2010; accepted 22 October 2010; posted 26 October 2010 (Doc. ID 131471); published 2 December 2010

To the best of our knowledge, proposed for the first time is the design of an optically broadband variable photonic delay line (VPDL) using an electronically controlled variable focus lens (ECVFL), mirror motion, and beam-conditioned free-space laser beam propagation. This loss-minimized fiber-coupled VPDL design using micro-optic components has the ability to simultaneously provide optical attenuation controls and analog-mode high-resolution (subpicoseconds) continuous delays over a moderate (e.g., <5 ns) range of time delays. An example VPDL design using a liquid-based ECVFL demonstrates up to a 1 ns time-delay range with >10 dB optical attenuation controls. The proposed VPDL is deployed to demonstrate a two-tap RF notch filter with tuned notches at 854.04 and 855.19 MHz with 22.6 dB notch depth control via VPDL attenuation control operations. The proposed VPDL is useful in signal conditioning applications requiring fiber-coupled broadband light time delay and attenuation controls. © 2010 Optical Society of America

OCIS codes: 230.0230, 350.4010, 060.2310, 060.5625.

1. Introduction

The subject of variable photonic delay lines (VPDLs) has been a key area in photonics research with VPDL applications that include phased-array antenna controls, RF transversal filtering, all-optical signal processing and communication systems, and laser-interferometry and low-coherence reflectometry (or optical coherence tomography) metrology and sensing systems. Various VPDL designs using different bulk, integrated, and fiber technologies have been proposed in the past for ultrashort-, short-, medium-, and long-range optical signal delays [1–5]. Free-space [6,7] and wavelength-sensitive optical fiber [8–18] and integrated-optic waveguide ring resonator-based [19,20] VPDL designs have been proposed for varying time-delay dynamic ranges of operation. A major advantage of a free-space optical delay line design is that it does not have the temporal spreading effect of the broadband optical signal that happens due to the inherently dispersive properties of an optical fiber delay medium. A fixed grating within a free-space delay geometry using a rotating mirror to select the broadband time delay has also been proposed, although with limited (e.g., <100 ps) delays and a restricted fiber interconnect coupling [21]. Do note that, for very short fiber delays, the fiber dispersion effect can be low and compensated by dispersion-shifted fiber, although within a limited spectral bandwidth limit for the optical signal requiring the broadband time delay. The limitation with prior-art [22] fiber-coupled free-space moving-mirror (or optic) delay lines is that when the mirror (or optic) is translated to change the delay of the optical beam, the light coupled back into the input/output single-mode fiber (SMF) and the RF modulator optics suffer a strong and varying loss that greatly limits the delay range of the VPDL to short (e.g., 300 ps) delays. Specifically, SMF optical coupling loss ramps up

0003-6935/10/356718-08$15.00/0

quickly due to nonlinear Gaussian beam waist expansion to over 30 dB [23–25]. Most RF and all-optical signal processing applications using broadband light require delays in excess of 100 ps and, hence, one would ideally desire an optically broadband VPDL that essentially eliminates the large free-space-SMF optical coupling loss and works over 300 ps delays and into the several nanoseconds regime. Thus, this paper presents, for the first time to the best of our knowledge, such a desired VPDL, which is formed using the concept of an electronically agile lens-based free-space broadband low-loss VPDL. The paper describes the optical design of the novel agile lens-based VPDL and experimentally verifies its operation in the RF and optical domains. Also demonstrated is a two-tap RF-tunable nulling filter using the proposed VPDL. Note that the power of an electronically controlled variable focus lens (ECVFL), such as a liquid-crystal ECVFL, has been earlier proposed and demonstrated for fiber-to-free-space-fiber optical interconnect applications [26,27], including the use of an ECVFL as an alignment tweaker within a liquid-crystal delay line unit [28]. Additionally, ECVFL micro-optic technology has been shown to be highly versatile in designing telecommunication, metrology, and sensor modules [29–35]. In this paper, deployed, for the first time to the best of our knowledge, is liquid lens technology for designing a broadband VPDL.

2. Proposed Agile Lens-Based Variable Photonic Delay Line Design

The design of the proposed agile lens-based VPDL is shown in Fig. 1. The delay line uses an interconnection SMF, a fiber lens (FL), an ECVFL, a flat mirror M, and an external fiber-optic circulator C. The micro-optical fiber lens and mirror components are placed in a narrow tube with the mirror motion controlled by mechanical, electromechanical, or electromagnetic means. Depending on the mirror actuation technology used and the maximum length of the tube, the VPDL delay reset time can range from milliseconds to a few seconds. Typically, ECVFL technology (e.g., LC, liquid, deformable mirror membrane) can also be reset in a few milliseconds to seconds. Thus, the present VPDL design is suited for applications where delay reset speed is not a premium priority but where precision and range of broadband delay is of importance (e.g., RF and optical metrology and testing applications).

Light enters the VPDL through the input IN port which is connected to an FL via an SMF. At a distance $2d_1$ from the FL, the Gaussian beam expands to a waist that is equal to the beam waist $2w_1$ at the exit aperture of the FL. This $2d_1$ distance is referred to as the self-imaging distance of a fiber lens [16]. The ECVFL is placed at this FL self-imaging plane. The diverging beam into the ECVFL is focused back by the ECVFL, thus forming a minimum beam waist $2w_{\mathrm{Min}}$ at a distance d_2 from the ECVFL. This d_2

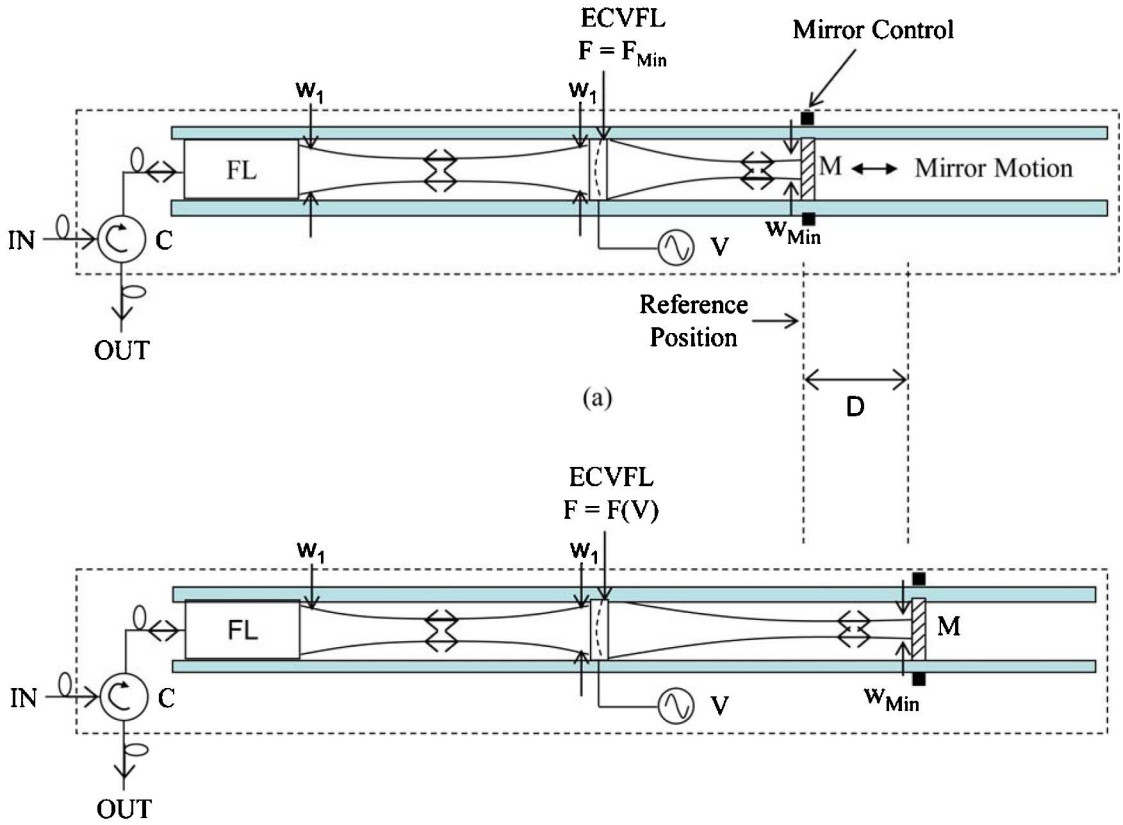

Fig. 1. (Color online) Proposed optically broadband VPDL using an ECVFL.

distance depends on the tuned focal length of the ECVFL. Depending on the ECVFL focal length F, the mirror M is positioned at the minimum beam waist plane such that the minimum beam spot forms on M. This alignment arrangement ensures that the reflected beam exactly traces the path of the incoming beam and couples back into the FL with essentially no SMF–free-space coupling losses. The ECVFL focal length satisfying this low loss coupling condition for a given mirror motion of D_1 is called F_{Ideal}. Thus, the requirement for the proposed folded optical system to form a minimum beam waist at M for ideally lossless operation has been exploited to propose the low loss free-space VPDL using agile lensing. By moving the mirror M and adjusting F, a lossless FL coupling condition is achieved for different mirror positions. The mirror motion constitutes broadband optical signal delay and the VPDL operation.

Figure 1(a) shows the zero reference delay setting of the proposed VPDL. The ECVFL is set to its minimum focal length F_{Min} (i.e., strongest lensing), and hence the minimum beam waist $2w_{\text{Min}}$ is formed nearest to the ECVFL. Next, as shown in Fig. 1(b), the ECVFL focal length F is varied to larger focal length values and the minimum beam waist is pushed farther away from the ECVFL. This additional distance D_1 with respect to the zero delay reference position (at $F = F_{\text{Min}}$) causes the optical signal to travel a greater distance. This additional time delay ΔT is given by

$$\Delta T = \frac{2D_1}{v_{\text{Air}}}, \tag{1}$$

where v_{Air} is the velocity of light in air. The Gaussian beam propagation analysis conducted next shows the design calculation of the minimum beam waist location for different values of F and the time-delay dynamic range of the VPDL. A Gaussian beam optical field can be represented by the complex q parameter $q(z)$ such that [36]

$$E(r,z) \propto \exp(jkr^2/2\, q(z)), \tag{2}$$

$$\frac{1}{q(z)} = \frac{1}{R(z)} - j\frac{\lambda}{\pi w^2(z)}. \tag{3}$$

Here, λ is the wavelength, $k = 2\pi/\lambda$, and $r = \sqrt{x^2 + y^2}$, where (x,y) are the Cartesian coordinates of the optical field plane, q_1 is the Gaussian beam q parameter at the location of the minimum waist radius, z is the optical beam travel direction, w is the $1/e^2$ beam radius, and R is the radius of curvature of the Gaussian beam wavefront. Using Eq. (3) with $R(z) = \infty$ and beam waist radius w_{Min1} at a distance d_1 before the ECVFL, the q parameter is given by

$$q_1 = \frac{\pi w_{\text{Min1}}^2}{\lambda} j. \tag{4}$$

Therefore, the q parameter q_2 of the beam at distance d_2 after passing through the ECVFL is given by

$$q_2 = \frac{Aq_1 + B}{Cq_1 + D}. \tag{5}$$

Here, A, B, C, and D are the elements of the ABCD matrix involving the beam transmission through the ECVFL and its subsequent propagation for a distance d_2 until it gets to a minimum beam waist $2w_{\text{Min}}$. In other words, one can write the matrix as

$$\begin{bmatrix} A & B \\ C & D \end{bmatrix} = \begin{bmatrix} 1 & d_2 \\ 0 & 1 \end{bmatrix} \times \begin{bmatrix} 1 & 0 \\ -\frac{1}{F} & 1 \end{bmatrix} \times \begin{bmatrix} 1 & d_1 \\ 0 & 1 \end{bmatrix}, \tag{6}$$

where F is the focal length of the positive focus ECVFL.

$$\Rightarrow \begin{bmatrix} A & B \\ C & D \end{bmatrix} = \begin{bmatrix} 1 & d_2 \\ 0 & 1 \end{bmatrix} \times \begin{bmatrix} 1 & d_1 \\ -\frac{1}{F} & 1 - \frac{d_1}{F} \end{bmatrix}, \tag{7}$$

$$\Rightarrow \begin{bmatrix} A & B \\ C & D \end{bmatrix} = \begin{bmatrix} 1 & d_2 \\ 0 & 1 \end{bmatrix} \times \begin{bmatrix} M_1 & M_2 \\ M_3 & M_4 \end{bmatrix}, \tag{8}$$

$$\Rightarrow \begin{bmatrix} A & B \\ C & D \end{bmatrix} = \begin{bmatrix} M_1 + d_2 M_3 & M_2 + d_2 M_4 \\ M_3 & M_4 \end{bmatrix}, \tag{9}$$

From Eqs. (3) and (5), one can write

$$\frac{1}{q_2} = \frac{1}{R_2} - j\frac{\lambda}{\pi w^2(d_2)} = \frac{Cq_1 + D}{Aq_1 + B}. \tag{10}$$

When a minimum beam waist forms at a distance d_2, then the complex q parameter satisfies the condition

$$\text{Re}\left(\frac{1}{q_2}\right) = 0. \tag{11}$$

Here "Re" denotes the real part of the complex quantity. Solving Eq. (11), one gets a relationship between d_2 and F. This is given as

$$d_2 = \frac{-M_2 M_4 - M_1 M_3 \left(\frac{\pi w_{\text{Min1}}^2}{\lambda}\right)^2}{M_4^2 + M_3^2 \left(\frac{\pi w_{\text{Min1}}^2}{\lambda}\right)^2}. \tag{12}$$

In Eq. (12), the only variable on the right-hand side of the equation is F, given that w_{Min1}, λ, and d_1 are known. Hence the free-space distance change dynamic range R of the VPDL is given by

$$R = d_{2\,\mathrm{Max}} - d_{2\mathrm{Min}}, \tag{13}$$

where $d_{2\,\mathrm{Max}}$ and $d_{2\,\mathrm{Min}}$ are the values of d_2 at $F = F_{\mathrm{Max}}$ and $F = F_{\mathrm{Min}}$, respectively. F_{Max} and F_{Min} are the maximum and minimum ECVFL focal lengths, respectively. Hence, the time-delay dynamic range R_T of the VPDL is given by

$$R_T = \frac{2(d_{2\,\mathrm{Max}} - d_{2\,\mathrm{Min}})}{v_{\mathrm{Air}}}. \tag{14}$$

3. Experimental Demonstration of the Agile-Lens Based VPDL

The proposed VPDL in Fig. 1 is experimentally demonstrated using a Varioptic Arctic 320 electrowetting technology liquid lens, an IR 1550 nm laser source, and a $2d_1 = 12.5$ cm self-imaging FL with $2w_{\mathrm{Min1}} = 500$ μm. A movable IR mirror is placed on a mechanical rail such that the mirror assembly can slide on the rail to change mirror positions and, hence, time delay. To show input optical signal delay, the IR light from the laser source is intensity modulated at 500 MHz using an integrated-optic electro-optic RF modulator. Light exiting through the VPDL OUT port is demodulated using a Nortel Networks high-speed photodetector, thus retrieving the delayed RF signal. To emphasize the importance of using an ECVFL to form a loss minimized free-space delay line, Fig. 2 shows the comparison between the optical power levels at the output port of the VPDL when F is set to F_{flat} or F at an infinity state that is equivalent to having no ECVFL in the optical beam path and when F is set to F_{Ideal}, i.e., when the agile beam control is implemented via the ECVFL. Figure 2 sample delay positions for the mirror are (a) $D_1 = 0$ cm, (b) 5 cm, and (c) 10 cm with the difference in output optical power levels are 11.2, 12.5, and 13.7 dB, respectively. Thus, light couples back efficiently into the FL when $F = F_{\mathrm{Ideal}}$ for different mirror positions. The light coupling efficiency into the SMF for each mirror position can also be controlled via ECFVL F control to form an inherent variable optical attenuator (VOA) with the VPDL structure. As shown in Fig. 2, optical VOA control of >10 dB is possible for the demonstrated VPDL.

Note that the maximum value of D_1 using the deployed liquid lens is $R = 16.2$ cm as determined using Eq. (13) with $w_{\mathrm{Min1}} = 0.69$ mm, $F_{\mathrm{Min}} = 4.9$ cm, and $F_{\mathrm{Max}} = 21.1$ cm. The F_{Min} and F_{Max} values used for the ECVFL are for the specific Varioptic liquid lens used in the experiment. Hence, the maximum D_1 for the experiment was chosen to be 15 cm. The time-delay range is calculated using Eq. (14) and, for the given liquid ECVFL, is $R_T = 1.08$ ns. Hence, Fig. 3 shows the oscilloscope traces of the delayed RF signals for mirror positions of $D_1 = 5$, 10, and 15 cm, corresponding to RF signal delays of 1/3, 2/3, and 1 ns, respectively. The lower curve in each plot shows that the VPDL provided a 500 MHz signal for the $D_1 = 0$ reference mirror position, while the upper curves shows the RF signal relative to the reference delay position. Each Fig. 3 oscilloscope photograph is

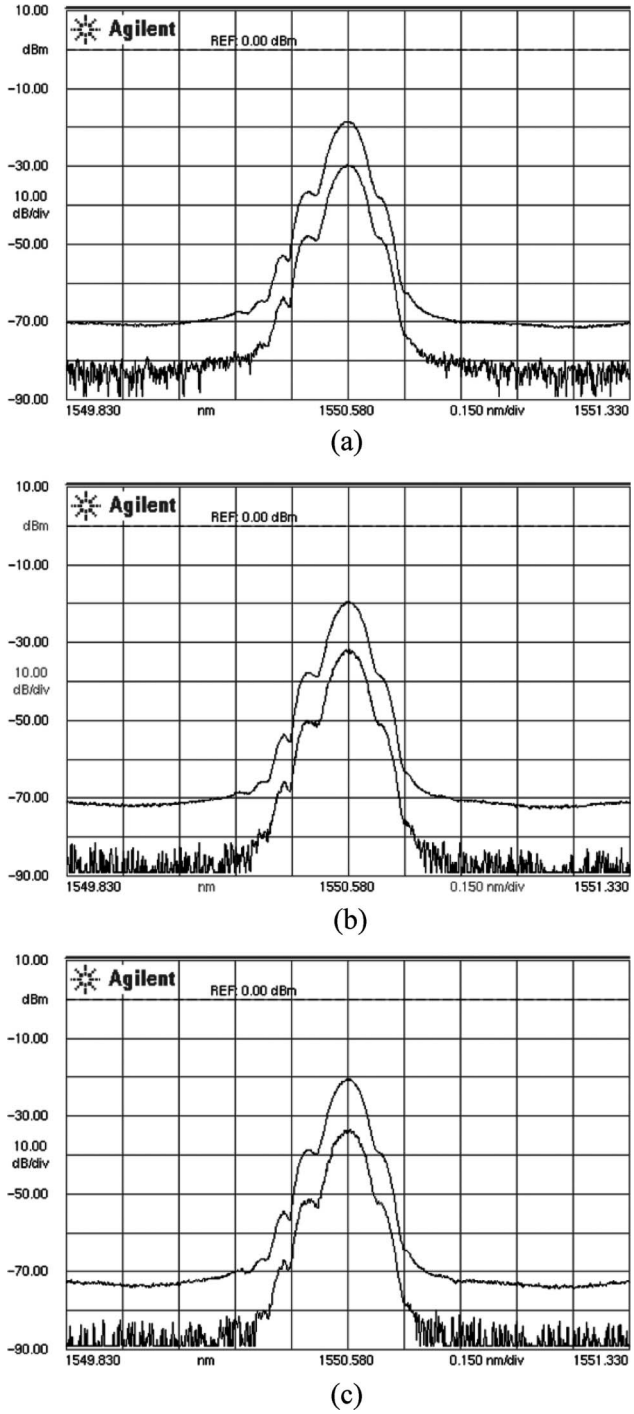

Fig. 2. The top curve shows the maximum optical power processed via the ECVFL-based VPDL for the specified mirror (delay) location with the ECVFL set at $F = F_{\mathrm{ideal}}$ for ideal low-loss SMF-lens coupling. The bottom curve is produced when the ECVFL focal length is set to $F = 0$ (i.e., unaided beam control) for the given mirror/delay location, indicating the >10 dB higher coupling loss in the VPDL. (a) At the zero delay mirror position, a 11.21 dB improvement, (b) with a 5 cm delay, a 12.52 dB improvement, and (c) with a 10 cm delay, a 13.73 dB improvement in optical coupling achieved over the ECVFL state $F = 0$.

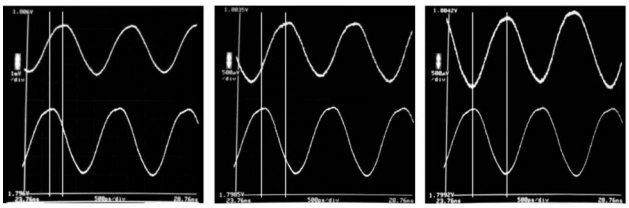

Fig. 3. Oscilloscope traces showing a 500 MHz RF signal delayed via the proposed ECVFL-based VPDL with relative delays of (a) 1/3 ns, (b) 2/3 ns, and (c) 1 ns. Bottom trace is the reference RF signal. Time scale is 0.5 ns/div.

marked with two white vertical lines. One vertical white line (at the left side of each photo) is aligned with a peak of the bottom reference RF signal. The other white line (at the right side of the photo) is aligned with the peak of the time-delayed RF signal and shows the changing RF time delay (vertical white line moves left to right for signal trace) due to the electrically controlled VPDL. The time-delay resolution of the proposed VPDL is limited by the mirror motion control actuator performance and can be under 1 ps using precision piezoelectric motion stages [37].

Figure 4 shows the C band (1530–1550 nm) broadband response of the VPDL for an example mirror position of $D_1 = 15$ cm. As seen in Fig. 4, the measured spectral variation for the given wavelength band is ± 0.2 dB and is caused by Fabry–Perot response from the uncoated surfaces of the liquid lens. The ECVFL transmission loss is measured to be 3.5 dB for the C band. As the optical beam is made to pass through the ECVFL twice in the VPDL, the total ECVFL loss is measured to be 7 dB. The single-pass loss of the FL is measured to be 0.65 dB; hence the total FL loss within the demonstrated VPDL is 1.3 dB. The FL-to-free-space-to-FL coupling loss for the experiment is 0.5 dB. The circulator port1–port2 loss is 0.6 dB and port2–port3 loss is measured to be 0.6 dB. Hence, the total loss for the demonstrated VPDL is 10 dB. This relatively high loss for the experimental VPDL is dominated by the ECVFL loss, as the deployed ECVFL is designed for use in the visible optical wavelengths (400–700 nm), where it has a 92% transmission or 0.5 dB loss. With proper IR antireflection (AR) coating on the ECVFL, the IR single-pass ECVFL loss is expected to be 0.5 dB, and this reduces ECVFL-caused total loss from 7 to 1 dB when the IR beam is passed through the ECVFL twice. Today, a high-quality FL has a single-pass loss of 0.1 dB. Similarly, an excellent commercial circulator has a 0.4 dB port-to-port (port1–port2 and port2–port3) loss. Hence, by employing an IR AR-coated ECVFL with optimized FL–free-space–FL coupling of 0.1 dB and the best FL and circulator, the total expected VPDL loss will be a reasonable 2.1 dB. In effect, compared to a typical free-space VPDL design for a 1 ns delay with a maximum loss >15 dB [23], the proposed delay line has the potential for a much improved 2.1 dB loss. Note that a broadband mirror-based ECVFL can also be used in the proposed VPDL, which leads to an even lower-loss (e.g., <1 dB) VPDL design, given that mirror coatings can be highly low loss. Specifically, as shown in Fig. 5, an optimal-component-count broadband VPDL design is possible where a deformable mirror M performs the function of both the movable mirror for time delay control as well as the ECVFL for optical beam focus control. Note that short fiber interconnection lengths and broadband optical

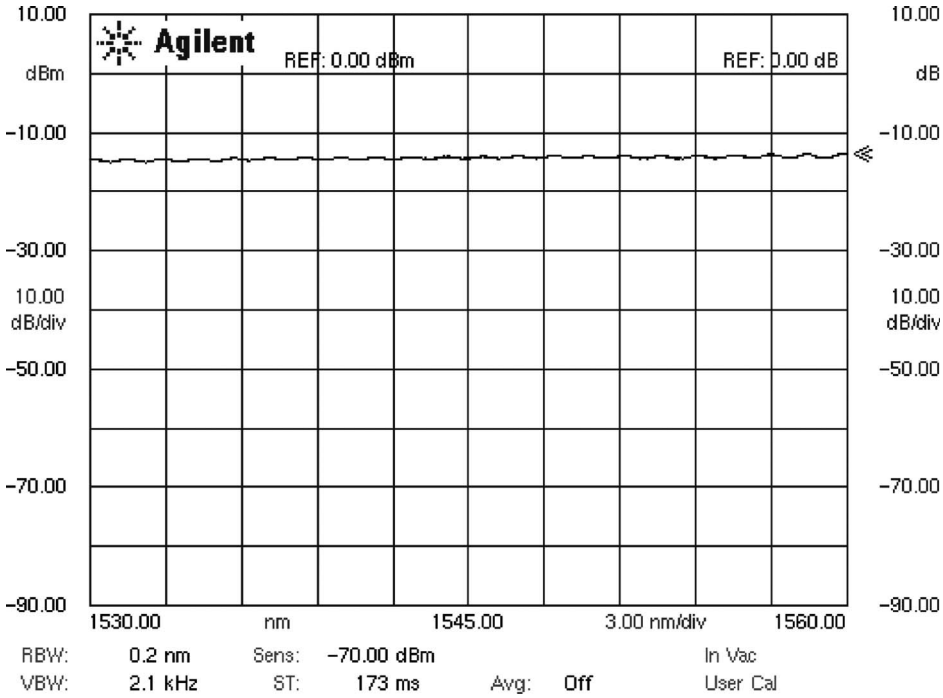

Fig. 4. Broadband optical response of the ECVFL-based VPDL with mirror position at $D = 15$ cm and $F = F_{\text{ideal}}$.

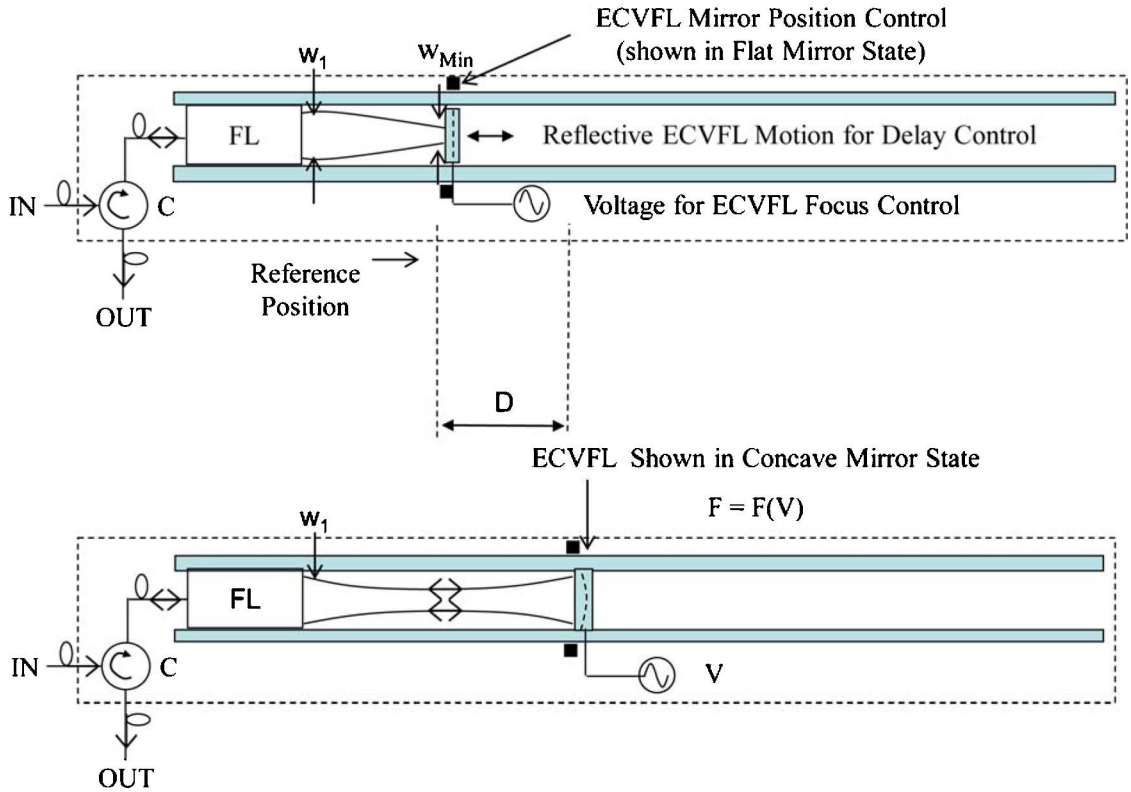

Fig. 5. (Color online) Proposed optically broadband VPDL using an a deformable mirror (DM) that acts both as a moving mirror for time-delay control and a reflective ECVFL for beam focus controls.

circulators should be deployed in the proposed VPDL to keep optical dispersion effects to a minimum.

The proposed VPDL design gets its compactness from its small cross section, corresponding to typical micro-optic diameters of under 5 mm. As shown in Figs. 1 and 5, the VPDL module is like a narrow long package, much like a pen. Because one can also use folding optics like a total internal reflection (TIR) prism, one can fold the delay path to shorten the VPDL package length. For the design example demonstrated and using one TIR prism for path length folding, the package length can be under 25 cm with a 1 cm cross section. It is possible to envision microelectromechanical-systems-technology-based compact bench packaging for the proposed VPDL to further miniaturize the package size [38].

As an application example, the demonstrated VPDL is used to design a two-tap RF nulling filter.

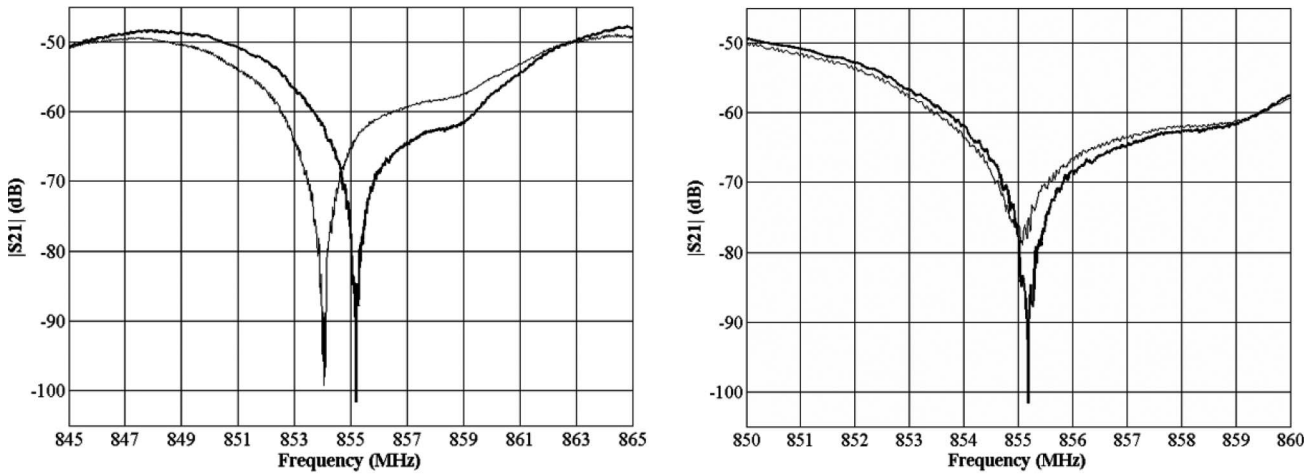

Fig. 6. RF network analyzer response of the demonstrated two-tap RF notch filter using the proposed VPDL as one arm of the tap delay. (a) Shown is RF notch frequency tuning (scale of 2 MHz/div) from 854.04 to 855.19 MHz via fine mirror motion of 13 mm in the VPDL. (b) Shown is a 22.6 dB change in notch depth at 855.19 MHz (scale of 1 MHz/div) implemented by change of ECVFL focal length that leads to the required optimal RF tap signal attenuation control.

Tuning of the null frequency is implemented by changing the RF time delay via the demonstrated VPDL. Notch depth control is implemented using the inherent RF VOA mechanism in the VPDL. The reference tap used to make the filter comes from the RF network analyzer internal tunable RF source that also drives the VPDL via an RF-to-optical integrated-optic modulator. The time-delayed optical signal is recovered as a delayed RF signal by the high-speed photodetector and then fed to an electronic adder to produce the two-tap filter with multiple null frequencies located at $f_{\text{null}} = (2\,k + 1)f_0$ with the fundamental null frequency $f_0 = 1/2\tau$ and $k = 0, 1, 2, \ldots$, indicating the different null positions in the processed output RF spectrum [39]. Here, τ is the relative delay between the two RF signals that are added via the electrical adder. Figure 6(a) shows the RF spectrum response of the VPDL-based RF filter, with the observed RF notch being tuned from 854.04 and 855.19 MHz, using a 13 mm mirror motion (or $\delta\tau =$ 43.33 ps) within the VPDL and using a $\tau = 32.18$ ns with $k = 27$. Figure 6(b) shows a 22.6 dB notch depth control using the VOA control in the VPDL that matches the two RF tap weights to produce the deepest RF null.

4. Conclusion

In conclusion, presented for the first time to the best of our knowledge is a loss-minimized broadband free-space VPDL using electronically controlled agile lensing. The proposed design uses the electronic tuning capability of the agile lens to implement a controlled loss free-space-to-fiber lens coupling mechanism for the changing mirror distances required for variable delay control. In addition, the VPDL contains an inherent VOA formed via the ECVFL controls for free-space beam focus change. The proposed basic VPDL is experimentally demonstrated for a 1 ns delay range with >20 dB RF attenuation controls shown in a two-tap RF nulling filter implementation. The proposed micro-optic-design-based VPDL can be a useful compact delay and gain control module in applications using broadband light, such as in optical/RF radar controls, tunable optical/RF filters, and ultrashort pulse laser systems and related signal processors for metrology.

References

1. N. A. Riza, ed., *Selected Papers on Photonic Control Systems for Phased Array Antennas*, Vol. MS136 of SPIE Milestone Series (SPIE, 1997).
2. R. A. Minasian, "Photonic signal processing of microwave signals," IEEE Trans. Microwave Theory Tech. **54**, 832–846 (2006).
3. A. J. Seeds and K. J. Williams, "Microwave photonics," J. Lightwave Technol. **24**, 4628–4641 (2006).
4. J. Capmany and D. Novak, "Microwave photonics combines two worlds," Nat. Photon. **1**, 319–330 (2007).
5. J. P. Yao, "Microwave photonics," J. Lightwave Technol. **27**, 314–335 (2009).
6. N. Madamopoulos and N. A. Riza, "Demonstration of an all-digital 7 bit 33-channel photonic delay line for phased-array radars," Appl. Opt. **39**, 4168–4181 (2000).
7. D. Dolfi, P. Joffre, J. Antoine, J. P. Huignard, D. Philippet, and P. Granger, "Experimental demonstration of a phased-array antenna optically controlled with phase and time delays," Appl. Opt. **35**, 5293–5300 (1996).
8. X. S. Yao and L. Maleki, "A novel 2-D programmable photonic time delay device for millimeter wave signal processing applications," IEEE Photon. Technol. Lett. **6**, 1463–1465 (1994).
9. A. P. Goutzoulis, D. K. Davies, and J. M. Zomp, "Prototype binary fiber optic delay line," Opt. Eng. **28**, 1193–1202 (1989).
10. R. A. Soref, "Fiber grating prism for true time delay beam steering," Fiber Integr. Opt. **15**, 325–333 (1996).
11. R. D. Esman, Y. Frankel, J. L. Dexter, L. Goldberg, M. G. Parent, D. Stilwell, and D. G. Cooper, "Fiber-optic prism true time delay antenna feed," IEEE Photon. Technol. Lett. **5**, 1347–1349 (1993).
12. R. A. Minasian, "Photonic signal processing of high-speed signals using fiber gratings," Opt. Fiber Technol. **6**, 91–108 (2000).
13. J. Capmany, D. Pastor, and B. Ortega, "New and flexible fiber-optic delay-line filters using chirped Bragg gratings and laser arrays," IEEE Trans. Microwave Theor. Tech. **47**, 1321–1326 (1999).
14. V. Polo, B. Vidal, J. L. Corral, and J. Marti, "Novel tunable photonic microwave filter based on laser arrays and $N \times N$ AWG-based delay lines," IEEE Photon. Technol. Lett. **15**, 584–586 (2003).
15. N. A. Riza, M. A. Arain, and S. A. Khan, "Hybrid analog-digital variable fiber-optic delay line," J. Lightwave Technol. **22**, 619–624 (2004).
16. N. A. Riza, "Switchless hybrid analog-digital variable optical delay line for radio frequency signal processing," Opt. Eng. **48**, 035005 (2009).
17. P. Q. Thai, A. Alphones, and D. R. Lim, "Limitations by group delay ripple on optical beam-forming with chirped fiber grating," J. Lightwave Technol. **27**, 5619–5625 (2009).
18. B. M. Jung and J. P. Yao, "A two-dimensional optical true time-delay beamformer consisting of a fiber Bragg grating prism and switch-based fiber-optic delay lines," IEEE Photon. Technol. Lett. **21**, 627–629 (2009).
19. G. Lenz, B. J. Eggleton, C. K. Madsen, and R. E. Slusher, "Optical delay lines based on optical filters," IEEE J. Quantum Electron. **37**, 525–532 (2001).
20. A. Meijerink, C. G. H. Roeloffzen, R. Meijerink, L. Zhuang, D. A. I. Marpaung, M. J. Bentum, M. Burla, J. Verpoorte, P. Jorna, A. Hulzinga, and W. van Etten, "Novel ring resonator-based integrated photonic beamformer for broadband phased array receive antennas—part I: design and performance analysis," J. Lightwave Technol. **28**, 3–18 (2010).
21. G. J. Tearney, B. E. Bouma, and J. G. Fujimoto, "High-speed phase- and group-delay scanning with a grating-based phase control delay line," Opt. Lett. **22**, 1811–1813 (1997).
22. "OZ optics," Canada ODL-100, ODL-200 Datasheets (2010).
23. S. Yuan and N. A. Riza, "General formula for coupling loss characterization of single mode fiber collimators by use of gradient-index rod lenses," Appl. Opt. **38**, 3214–3222 (1999).
24. S. Yuan and N. A. Riza, "General formula for coupling loss characterization of single mode fiber collimators by use of gradient-index rod lenses: errata," Appl. Opt. **38**, 6292 (1999).
25. M. van Buren and N. A. Riza, "Foundations for low-loss fiber gradient-index lens pair coupling with the self-imaging mechanism," Appl. Opt. **42**, 550–565 (2003).
26. N. A. Riza and M. C. DeJule, "Three terminal adaptive nematic liquid crystal lens device," Opt. Lett. **19**, 1013–1015 (1994).
27. N. A. Riza and M. C. DeJule, "A novel programmable liquid crystal lens device for adaptive optical interconnect

and beamforming applications," presented at the International Conference on Optical Computing, Edinburgh, Scotland, 22–25 August 1994.
28. N. A. Riza and S. Yuan, "Demonstration of a liquid crystal adaptive alignment tweeker for high speed infrared band fiber-fed freespace systems," Opt. Eng. **37**, 1876–1880 (1998).
29. S. A. Reza and N. A. Riza, "A liquid lens-based broadband variable fiber optical attenuator," Opt. Commun. **282**, 1298–1303 (2009).
30. S. A. Reza and N. A. Riza, "High dynamic range variable fiber optical attenuator using digital micromirrors and optofluidics," IEEE Photon. Technol. Lett. **21**, 845–847 (2009).
31. N. A. Riza and P. J. Marraccini, "Broadband 2 × 2 free-space optical switch using electrically controlled liquid lenses," Opt. Commun. **283**, 1711–1714 (2010).
32. N. A. Riza and S. A. Reza, "Non-contact distance sensor using spatial signal processing," Opt. Lett. **34**, 434–436 (2009).
33. M. Sheikh and N. A. Riza, "Motion-free hybrid design laser beam propagation analyzer using a digital micro-mirror device and a variable focus liquid lens," Appl. Opt. **49**, D6–D11 (2010).
34. N. A. Riza and S. A. Reza, "Smart agile lens remote optical sensor for three-dimensional object shape measurements," Appl. Opt. **49**, 1139–1150 (2010).
35. S. A. Reza and N. A. Riza, "Agile lensing-based non-contact liquid level optical sensor for extreme environments," Opt. Commun. **283**, 3391–3397 (2010).
36. H. Kogelnik and T. Li, "Laser beams and resonators," Appl. Opt. **5**, 1550–1567 (1966).
37. Piezo actuators, PI Catalog, 2010 (www.pi-usa.us).
38. T.-R. Hsu, ed., *MEMS Packaging* (INSPEC, IEE, 2004).
39. N. A. Riza and F. N. Ghauri, "High resolution tunable microwave filter using hybrid analog-digital controls via an acousto-optic tunable filter and digital micromirror device," J. Lightwave Technol. **26**, 3056–3061 (2008).